



HAL
open science

Experimental measurement and modelling of vapor-liquid equilibrium for 3,3,3- Trifluoropropene (R1243zf) and trans-1,3,3,3-Tetrafluoropropene (R1234ze(E)) binary system

Zhiqiang Yang, Alain Valtz, Christophe Coquelet, Jiangtao Wu, Jian Lu

► To cite this version:

Zhiqiang Yang, Alain Valtz, Christophe Coquelet, Jiangtao Wu, Jian Lu. Experimental measurement and modelling of vapor-liquid equilibrium for 3,3,3- Trifluoropropene (R1243zf) and trans-1,3,3,3-Tetrafluoropropene (R1234ze(E)) binary system. *International Journal of Refrigeration*, 2020, 120, pp.137-149. 10.1016/j.ijrefrig.2020.08.016 . hal-02963711

HAL Id: hal-02963711

<https://hal.science/hal-02963711>

Submitted on 11 Oct 2020

HAL is a multi-disciplinary open access archive for the deposit and dissemination of scientific research documents, whether they are published or not. The documents may come from teaching and research institutions in France or abroad, or from public or private research centers.

L'archive ouverte pluridisciplinaire **HAL**, est destinée au dépôt et à la diffusion de documents scientifiques de niveau recherche, publiés ou non, émanant des établissements d'enseignement et de recherche français ou étrangers, des laboratoires publics ou privés.

Experimental Measurement and Modelling of Vapor-Liquid Equilibrium for 3,3,3-Trifluoropropene (R1243zf) and trans-1,3,3,3-Tetrafluoropropene (R1234ze(E)) Binary System

Zhiqiang Yang^{a,c}, Alain Valtz^b, Christophe Coquelet^{b*}, Jiangtao Wu^a, Jian Lu^c

^a Key Laboratory of Thermo-Fluid Science and Engineering, Ministry of Education, Xi'an Jiaotong University, Xi'an, 710049, China

^b Mines Paristech, PSL University, CTP -Centre of Thermodynamics of Processes, 35 rue Saint-Honoré, 77300 Fontainebleau, France

^c State Key Laboratory of Fluorine & Nitrogen Chemicals, Xi'an Modern Chemistry Research Institute, Xi'an, 710065, China

*Corresponding author. E-mail address: christophe.coquelet@mines-paristech.fr. Telephone: +33164694962

Abstract

The environmental performance becomes the critical factor of the selection of refrigerant. 3,3,3-trifluoropropene (R1243zf) and trans-1,3,3,3-tetrafluoropropene (R1234ze(E)) are environmental friendly candidates to replace R134a. Whereas, in the consideration of environmental factor, safety, and energetic efficiency at the same time, none of the pure refrigerants has been proved to be a suitable solution. Mixed refrigerants provide an approach to this problem because the characteristics of refrigerant blends can be optimized for particular applications in the way pure component refrigerant alone cannot be. The purpose of this work is to explore an R1243zf/R1234ze(E) blend which can be possibly used as a long-term alternative to replace hydrofluorocarbons (HFCs) and hydrochlorofluorocarbons (HCFCs). We report the measurements of saturated vapor pressures of R1234ze(E) and R1243zf ranging from 273.17 to 353.13 K, and isothermal vapor-liquid equilibrium of R1243zf + R1234ze(E) systems from 283.15 to 323.14 K. The measurements are performed by static-analytic type apparatus coupled with two electromagnetic capillary samplers (ROLSI[®], patent of Armines). The experimental data are correlated by the Peng-Robinson (PR) equation of state (EoS) associated with Mathias-Copeman (MC) alpha function and classical mixing rules. For the comparison of conventional mixing rules and excess free

energy (G^E) mixing rules models, classic van der Waals one fluid mixing rules and modified Huron-Vidal second-order (MHV2) mixing rules are employed respectively to the correlation of experimental VLE data. The modeling results are in good agreement with the measured data, while the PRMC-MHV2 model exhibits better performance in VLE prediction.

Keywords:

Refrigerant blend, low-GWP alternatives, vapor-liquid equilibrium, modeling, HFOs

Nomenclature

Abbreviation

GWP	global warming potential	VLE	vapor-liquid equilibrium
HFOs	hydrofluoroolefins	vdW	van der Waals mixing rules
PR	Peng-Robinson equation of state	MHV2	modified Huron-Vidal second-order mixing rules
MC	Mathias-Copeman alpha function	NRTL	non-random two-liquid activity model
MRDP	average relative deviation of pressure	MAD _y	average absolute deviation of vapor-composition
BIAS	mean bias	R1234ze(E)	trans-1,3,3,3-tetrafluoropropene equation of state
R1243zf	3,3,3-trifluoropropen	EoS	

Roman

a	energy parameter of the equation of state	b	covolume parameter of the equation of state
G_m^E	excess Gibbs energy	q	coefficient of MHV2 mixing rule
N	number of data points	P	pressure (Pa)
R	molar gas constant (8.314472 J.mol ⁻¹ .K ⁻¹)	T	temperature (K)
u	Combined uncertainty	U	expanded uncertainty
x	liquid phase mole fraction	y	vapor phase mole fraction
n	molar mass	$m_{1,2,3}$	adjustable parameters
k_{ij}	binary interaction parameter	F	objective function
Z	compressor factor	H	enthalpy
v	molar volume		

Greek

α	Temperature dependent alpha function	τ	dimensionless interaction parameters
δ	relative deviation	Δ	absolute deviation
Δg_{ij}	interaction energy parameters of NRTL equation	ω	acentric factor
α_{12}	Relative volatility		

Subscripts

i, j	molecular species	c	critical property
calib	calibration	cal	calculated
exp	experimental	rep	repetability
m	mixture	r	reduce temperature

1 Introduction

Mitigating climate change is one of the biggest challenges facing humanity in this century. To address the issue, international climate conventions such as Montreal Protocol, Paris Agreement, F-Gas Regulations (European Parliament and The Council of the European Union, 2006), Kigali Agreement (UNEP, 2016), etc., have applied forms of regulation to eliminate greenhouse gas emissions. Hydrofluorocarbons (HFCs) and hydrochlorofluorocarbons (HCFCs), currently widely used saturated halohydrocarbon refrigerants, are scheduled to phase out because of their serious greenhouse effect on the climate. The refrigeration industry is trying to develop efficient alternative refrigerants with zero ozone depletion potential (ODP) and global warming potentials (GWP) lower than 150 as the requirement of G-gas regulation (European Parliament and The Council of the European Union, 2006). Hydrofluoroolefins (HFO) are unsaturated organic compounds composed of carbon, hydrogen, and fluorine (Wu et al., 2019). HFO usually exhibits zero ODP and extremely low GWP because of their specific molecular characteristics of owning a C=C double bond, being chlorine-free, and having a short atmospheric lifetime (González et al., 2015). Moreover, another important feature is that HFO and HFC have similar thermodynamic properties, consequently, HFOs are considered as the most promising alternatives.

Among them, 3,3,3-trifluoropropene (R1243zf) and trans-1,3,3,3-tetrafluoropropene (R1234ze(E)), two of alternative refrigerants with zero ODP, GWP less than 10, short atmospheric lifetime (González et al., 2015) and similar thermodynamic behavior as R134a, are recently promising candidates of R134a in air-conditioning and other applications under actual conditions. Until now, R1243zf and R1234ze(E) have been extensively studied from various aspects, such as thermodynamic properties, cooling performance in the refrigeration system. Brown et al. (2013) and Yang et al. (2019) carried out experimental studies on the saturated vapor pressure of R1243zf. The surface tension of R1243zf was measured by Kondou et al. (2015) at temperatures from 270 K to 360 K. Higashi et al. (2018a; 2018b) presented experimental data on vapor pressure, PVT properties, saturated liquid and vapor

densities, and critical parameters of R1243zf. Akasaka (2016) presented a Helmholtz energy EoS for R1243zf which valid for temperatures from 234 to 376 K and for pressures up to 35 MPa. Higashi et al. determined by (2010) the critical density and critical temperature of R1234ze(E) from the meniscus disappearing level as well as the intensity of the critical opalescence. Di Nicola et al. (2012) presented 78 vapor-pressure data of R1234ze(E) for temperatures from 223.1 to 353.1 K measured by two different laboratories. Qiu et al. (2013) conducted a density measurement of R1234ze(E) at pressures of up to 100 MPa and temperature from 283 to 363 K using a vibrating tube densimeter. Vapor pressure and saturated liquid density for R1234ze(E) were measured in the temperature range from 300 to 400 K by using the extraction method (Katsuyuki, 2016). The vapor pressures and ppT properties of R1234ze(E) ranging from 310 to 370 K, as well as isobaric specific heat capacity ranging from 310 to 370 K, were measured by Tanaka et al. (2010a; 2010b) using a metal-bellows calorimeter. Akasaka (2010) applied an extended corresponding states model for R1234ze(E) with typical uncertainties for vapor pressure, liquid density, and isobaric heat capacities (liquid and vapor) of 0.2%, 0.5%, and 5%, respectively. Ansari et al. (2020) performed a thermodynamic analysis on the vapor compression refrigeration system with dedicated mechanical subcooling using R1243zf as a refrigerant and compared its performance with R134a. Brown et al. (2014) investigate the heat transfer and pressure drop performance potentials of both R1234ze(E) and R1243zf and analyzes the effects of thermodynamic properties on the heat transfer and pressure drop performance.

The selection of the most suitable refrigerant is based on a number of criteria, including environmental considerations (low GWP, zero or near-zero ODP), safety (low toxicity, low flammability), and energetic performance (high efficiency, appropriate capacity) (Bobbo et al., 2018). Whereas, considering those criteria at the same time, no pure refrigerant is ideal in all regards because all of them have one or more negative attributes (McLinden et al., 2014). R1234ze(E) has low toxicity and mild flammability, however, it presents low cooling capacity, low coefficient of performance (COP), and low heat transfer performance than R32 and R134a (Longo et al., 2014; Mota-Babiloni et al., 2014). On the other hand, R1243zf is

flammable, even though it offers better cycle efficiency than those of the other R134a, R32, and R22 in air-conditioning cycles (Lai, 2014).

Mixed refrigerants provide an approach to this problem because the characteristics of refrigerant blends can be optimized for particular applications in the way pure component refrigerant alone cannot be. Numerous investigations on refrigerant blends have presented, and many of them focus on HFC/HFO blends (Bobbo et al., 2018; Boonaert et al., 2020). Indeed, Some HFC/HFO blends show good performance in the thermodynamic cycle and engineering application, such as R450A (Mota-Babiloni et al., 2015) and R448A (Mendoza-Miranda et al., 2016), whereas their GWP values are difficult to meet the requirements of less than 150. As the environmental pollution is becoming more and more serious, environmental performance becomes the critical factor of the selection of refrigerant. It is extremely necessary to research low GWP refrigerant blends. Therefore, the purpose of this article is to explore an R1243zf/R1234ze(E) blend which offers GWP less than 10 and can be possibly used as a long-term alternative of HFCs and HCFCs (European Parliament and The Council of the European Union, 2006).

Thermodynamic properties of refrigerants are crucial to evaluate their cycle performance and optimize the design of the refrigeration system. Among the thermodynamic properties, vapor-liquid equilibrium (VLE) is one of the most important thermodynamic properties in engineering applications, which can be used to calculate, for example, residual enthalpy and entropy. If we can combine the residual enthalpy and entropy with the enthalpy and entropy of ideal gas, then we have the access to calculate the enthalpy and entropy of the refrigerant which is essential to evaluate the cycle performance and optimize the design of the refrigeration and system. In this work, isothermal VLE of R1243zf + R1234ze(E) blend at four temperatures (283.15, 293.15, 313.15, 323.14) K, together with vapor pressures of R1234ze(E) and R1243zf ranging from (273.17 to 353.13) K, were measured by static-analytical method. Peng-Robinson (PR) equation of state (EoS) associate with Van der Waals one fluid mixing rules and modified Huron-Vidal second-order (MHV2) mixing rules are employed to correlate the experimental VLE data.

2 Experiment

2.1. The material

The 3,3,3- trifluoropropene, product name R1243zf, CAS number: 677-21-4, is supplied by Synquestlabs, and the mass purity of R1243zf is more than 99 %. Trans-1,3,3,3-tetrafluoropropene(R1234ze(E)), product name R1234ze(E), CAS number: 29118-24-9, is bought from Climalife, the purity of R1234ze(E) is 99.5 % volumetric. The purities of materials are given by the suppliers and verified by chromatographic analysis and used without further purification. Table 1 shows the sample purities in detail.

Table 1. Chemical information.

Chemical Name	CAS No.	Supplier	Mass fraction purity ¹
R1243zf	677-21-4	Synquestlabs	99 % mass fraction
R1234ze(E)	29118-24-9	Climalife	99.50% volumetric

¹ GC gas chromatograph

2.2. Apparatus

The vapor-liquid equilibrium measurement of the R1243zf + R1234ze(E) binary system was conducted by an apparatus based on the static-analytic method. The schematic diagram of the apparatus is illustrated in Figure 1, and it is similar to the apparatus developed at CTP Mines ParisTech (Juntarachat et al., 2014; Wang et al., 2019).

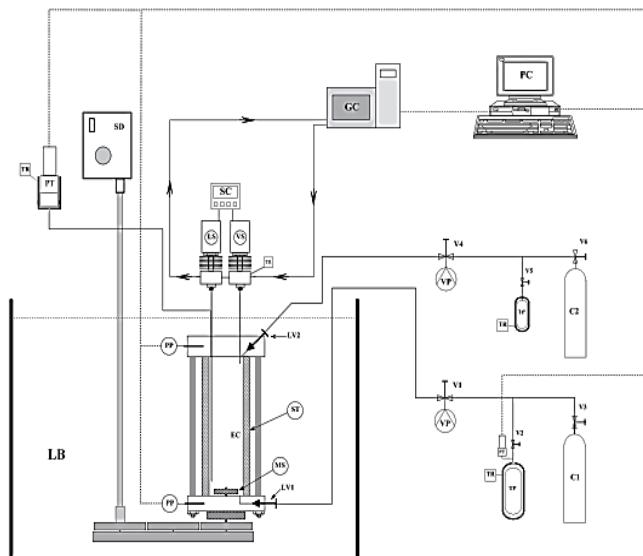


Figure 1. Schematic diagram of the apparatus.

EC: equilibrium cell; LV: loading valve; MS: magnetic stirrer, PP: platinum resistance thermometer probe; PT: pressure transducer; RT: temperature regulator; LB: liquid bath; TP: thermal press; C1: more volatile compound; C2: less volatile compound; V: valve; GC: gas Chromatograph; LS: liquid sampler; VS: vapor sampler; SC: sample controlling; PC: personal computer; VP: vacuum pump

One of the most important parts of the apparatus is the equilibrium cell, where the equilibrium of the binary component occurs. The equilibrium cell (around 30cm³) is made of a visually sapphire tube, as a consequence, the level of the liquid can be easily monitored. Two electromagnetic capillary samplers (ROLSI[®], patent of Armines) which can extract an infinitesimally small quantity of each phase without disturbing the equilibrium are installed at the top of the cell. The two ROLSIS[®], one for vapor sampling and the other for liquid sampling, are separately controlled by two time-relay controllers. For the sake of accelerating the equilibrium, a magnetic stirrer is installed inside the equilibrium cell through a hole in the bottom of the cell. The equilibrium cell is immersed in a thermostatic bath (LAUDA Proline RP3530) with an accuracy of 0.01 K.

To obtain more accurate temperature information inside the equilibrium cell, two platinum resistance thermometer probes (Pt100) are inserted inside the body of the equilibrium cell through two drilled holes, one in the top of the cell for vapor phase, the other in the bottom of the cell for liquid phase, which is connected to a data acquisition unit

(Agilent 34972A) and then the data is transmitted to the personal computer in real-time through an RS-232 interface. The two Pt100 probes are calibrated with a standard reference platinum resistance thermometer (SPRT25) probe (TINSLEY Precision Instruments), and the SPRT25 probe was calibrated by the Laboratoire National d'Essais (Paris) based on 1990 International Temperature Scale (ITS-90). The uncertainty of the temperature calibration is $u_{\text{calib}}(T) = 0.0006 \text{ K}$, within the range of 217.41K to 373.42K.

The pressure is measured using two pressure transducers, one for low pressure (DRUCK, Type PTX6100, 0-30 bar), one for high pressure (DRUCK, Type PTX6100, 0-300 bar). The two transducers are also connected to HP34970A which collect and transmit data to personal computer timely. In this work, the pressures inside the equilibrium cell are measured by the lower pressure transducer, which is calibrated a dead weight balance (DESGRANGES & HUOT) with a total measurement uncertainty to 0.002% of reading and pressure range available up to 1000 bar. Noteworthy, when the pressure transducer works, the temperature of pressure transducer should be regulated to a constant value with a heating cartridge via the PID regulator (WEST instrument, model 6100).

In general, the vapor pressure of investigated refrigerants maintains approximately 5 bar in a gas container at room temperature, however, for high-temperature VLE measurements, the working pressure usually higher than 5 bar. That makes difficult to load fresh experimental component into the equilibrium cell to acquire a new composition. To solve this problem, a thermal pressure cylinder (around 50 cm^3 , the maximum design pressure is 200 bar) is used to increase the pressure of an experimental component to the desired value. A certain quantity of the experimental component is first introduced into the pressure cylinder from the gas container, and the pressure cylinder is heated via a cartridge heater which is controlled by a temperature regulator. By modify the setting value of the temperature regulator, a pressure desired which is approximately 10 bar higher than the pressure of equilibrium cell can be acquired. Then, the experimental component is transferred to the equilibrium cell through the thermal pressure cylinder.

The compositions of mixtures are measured by gas chromatography. The infinitesimally

small quantity of samples in the equilibrium cell are extracted by ROLSI[®], and then the withdraw samples are transferred to gas chromatograph (GC) (ALPHA MOS, Type PR2100) and completely separated through the packed column, and eventually carried to the TCD by carrier gas. The information of the composition will be transformed into an electric signal in TCD. The gas chromatograph conditions are shown in Table 2.

Table 2. The gas chromatograph condition

GC Units	Conditions
Oven temperature	35 °C
Injector temperature	140 °C
Detector temperature	150 °C
Detector type	Thermal Conductivity Detector (TCD)
Carrier gas	Helium (245 kPa for TCD carrier; 105 kPa for reference carrier)
Gas chromatography column	RESTEK, 1 column: 5% KRYTOX, CBX-B 60/80, 3m*2mm

2.3. Operation procedure

At room temperature, the equilibrium cell and its loading lines are made under vacuum. The liquid bath is set to the temperature desired. When the equilibrium temperature is reached, a certain amount (approximately 5 cm³) of the heavier component is first loaded into the equilibrium cell. Then vapor pressure is measured at this temperature.

After that, a given amount of lighter component is introduced step by step to increase the pressure inside the cell, leading to successive equilibrium mixtures, in order to have enough points to cover the two-phase envelope (Valtz et al., 2019; Wang et al., 2019).

The equilibrium inside the cell is assumed to be reached when the pressure does not change during 10 minutes within ± 0.01 bar under continuous stirring. For each equilibrium condition, six or more samples of both vapor and liquid phases are taken using the ROLSI[®] and analyzed to verify the repeatability of the measurement.

3 Model and correlation

In this work, the Peng-Robinson (PR) equation of state (EoS)(Peng and Robinson, 1976),

one of the classical cubic equation, is utilized to model the experimental data. PR EoS is defined as Eq. 1.

$$p = \frac{RT}{v - b} - \frac{a(T)}{v^2 + 2bv - b^2} \quad 1$$

The parameters a and b are related to the critical pressure, critical temperature, and acentric factor as explained by Equations 2 and 3.

$$a = 0.45724 \frac{R^2 T_c^2}{p_c} \cdot \alpha(T) \quad 2$$

$$b = 0.07780 \frac{RT_c}{p_c} \quad 3$$

The original alpha function $\alpha(T)$ of PR EoS is given by Eq. 4.

$$\alpha(T) = \left[1 + (0.37464 + 1.54226\omega - 0.26992\omega^2)(1 - T_r^{1/2}) \right]^2 \quad 4$$

where ω is acentric factor, $T_r = T / T_c$, T and T_c represent reduce temperature and critical temperature. Critical properties of R1243zf and R1234ze(E) are taken from REFPROP 9.2 (Lemmon et al., 2013) and given in Table 3.

Table 3. Critical properties and regressed coefficient of Mathias-Copeman alpha function for R1243zf and R1234ze(E)

Components	Critical properties ¹			Regressed coefficients		
	T _c /K	P _c /MPa	ω	C ₁	C ₂	C ₃
R1243zf	376.93	3.5182	0.261	0.80529	-0.57580	1.64180
R1234ze(E)	382.51	3.6349	0.313	0.86178	-0.54007	2.33958

¹ resource taken from REFPROP 9.1 (Lemmon et al., 2013)

Here, we apply Mathias-Copeman (MC) alpha function(Mathias and Copeman, 1983) to replace the original alpha function of PR EoS to have a better performance for pure vapor pressure prediction, which is given by Eq. 5.

$$\alpha(T) = \left[1 + m_1 \left(1 - \sqrt{\frac{T}{T_c}} \right) + m_2 \left(1 - \sqrt{\frac{T}{T_c}} \right)^2 + m_3 \left(1 - \sqrt{\frac{T}{T_c}} \right)^3 \right] \quad 5$$

Where m_1 , m_2 , m_3 are three adjustable parameters fitted on the experimental data.

As for the mixing rules, there mainly exist conventional van der Waals (vdW) mixing rules and excess free energy (g^E) mixing rules. The vdW mixing rule is still attractive for refrigerant mixtures due to the simplicity and accuracy which mainly depend on the utilized interaction parameters. The g^E mixing rule is developed from theoretical basis and gives considerable accuracy in the description of VLE property for complex non-ideal mixtures(Orbey and Sandler, 1998). Therefore, in this study, vdW one fluid mixing rules (PR-MC-vdW) and one of classical g^E mixing rules, namely modified Huron-Vidal second-order (MHV2) mixing rules (PR-MC-MHV2) (Dahl and Michelsen, 1990), are employed to describe the VLE behavior of refrigerant mixture.

The vdW mixing rules are defined by Eq. 6.

$$\begin{aligned} a &= \sum_{i=1}^N \sum_{j=1}^N x_i x_j a_{ij} \\ a_{ij} &= (1 - k_{ij}) \sqrt{a_i a_j} \\ b &= \sum_{i=1}^N x_i b_i \end{aligned} \quad 6$$

where x_i is the mole fraction of component i , a_i is the energy parameter, and b_i is the covolume parameter of component i , and k_{ij} is the binary interaction parameter. N is the number of components of the system.

The MHV2 mixing rule can be written as Eq.7:

$$q_1 \left(\alpha_m - \sum_{i=1}^N x_i \alpha_{ii} \right) + q_2 \left(\alpha_m^2 - \sum_{i=1}^N x_i \alpha_{ii}^2 \right) = \frac{g_m^E}{RT} + \sum_{i=1}^N x_i \ln \left(\frac{b_m}{b_{ii}} \right) \quad 7$$

with

$$\alpha_m = \frac{\alpha_m}{b_m RT}; \quad \alpha_{ii} = \frac{\alpha_i}{b_i RT}; \quad b_m = \sum_{i=1}^N x_i b_i \quad 8$$

where $q_1 = -0.478$ and $q_2 = -0.0047$, as recommended by Michelsen (Dahl and Michelsen, 1990).

The NRTL (Renon and Prausnitz, 1968) model is used to calculate the excess Gibbs energy, for a binary system, the excess Gibbs energy of mixture g_m^E is determined by Eq.9.

$$\frac{g_m^E}{x_1 x_2 RT} = \frac{G_{21} \tau_{21}}{x_1 + x_2 G_{21}} + \frac{G_{12} \tau_{12}}{x_2 + x_1 G_{12}} \quad 9$$

With

$$G_{21} = \exp(-\alpha_{12} \tau_{12}); \quad G_{12} = \exp(-\alpha_{21} \tau_{21}) \quad 10$$

Where parameters α_{12} and α_{21} are non-randomness parameters, $\alpha_{21} = \alpha_{12}$, and α_{12} is usually set equal to 0.3 (Renon and Prausnitz, 1968) for VLE. Parameters τ_{21} and τ_{12} are the dimensionless interaction parameters, which are related to the interaction energy parameters Δg_{12} and Δg_{21} as formulated in Eq.11.

$$\tau_{12} = \frac{\Delta g_{12}}{RT}; \quad \tau_{21} = \frac{\Delta g_{21}}{RT} \quad 11$$

The binary interaction parameter k_{ij} of vdW mixing rule and interaction energy parameters Δg_{12} and Δg_{21} of NRTL equation are fitted on the VLE data of bubble pressure and vapor molar fraction according to the objective function given by Eq. 12.

$$F = \frac{100}{N} \left[\sum_i^N \left(\frac{p_{i,exp} - p_{i,cal}}{p_{i,exp}} \right)^2 + \sum_i^N \left(\frac{y_{i,exp} - y_{i,cal}}{y_{i,exp}} \right)^2 \right] \quad 12$$

Where N is the number of experimental data, $p_{i,exp}$ and $p_{i,cal}$ are the experimental and calculated bubble pressure, $y_{i,exp}$ and $y_{i,cal}$ are the experimental and calculated vapor-phase mole fraction.

4 Results and discussion

4.1. Vapour pressure

The vapor pressure of R1234ze(E) and R1243zf were measured at 15 temperature points from (288.05 to 357.86) K as listed in Table 4 and Table 5, and plotted in Figure 2.

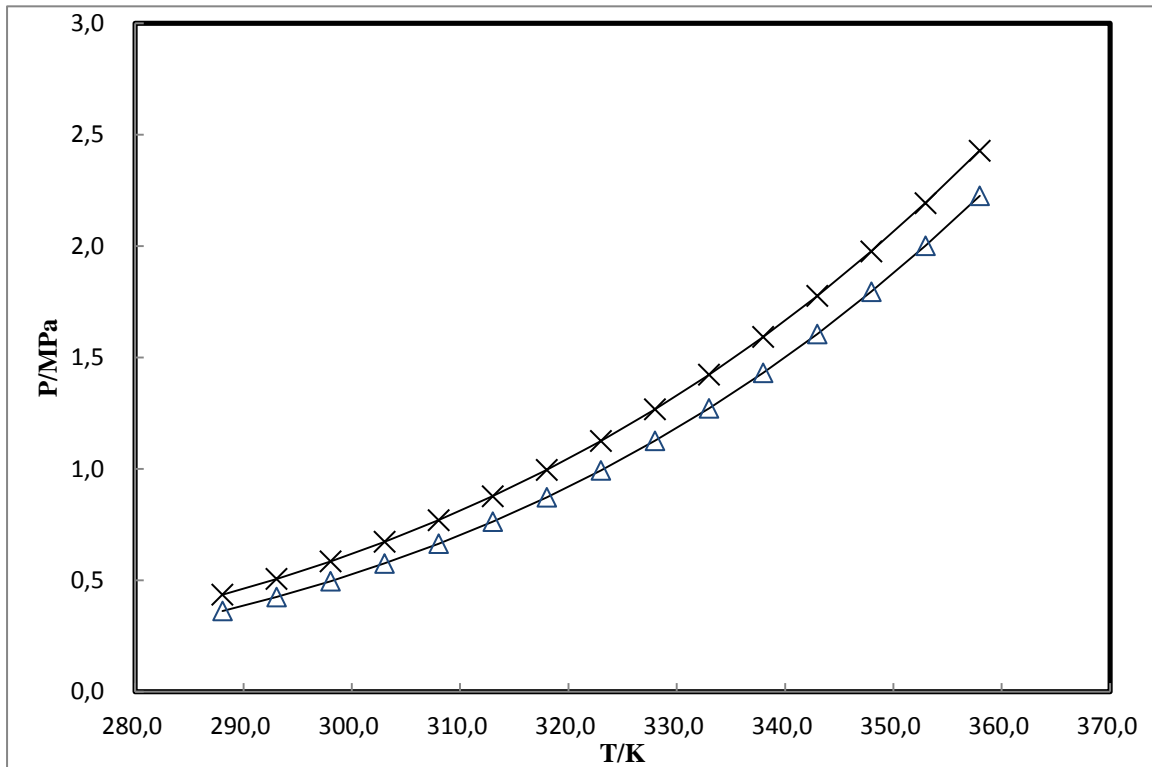


Figure 2. Experimental saturated pressures of R1243zf and R1234ze(E). (×): R1243zf; (Δ): R1234ze(E); solid line: PR-MC model.

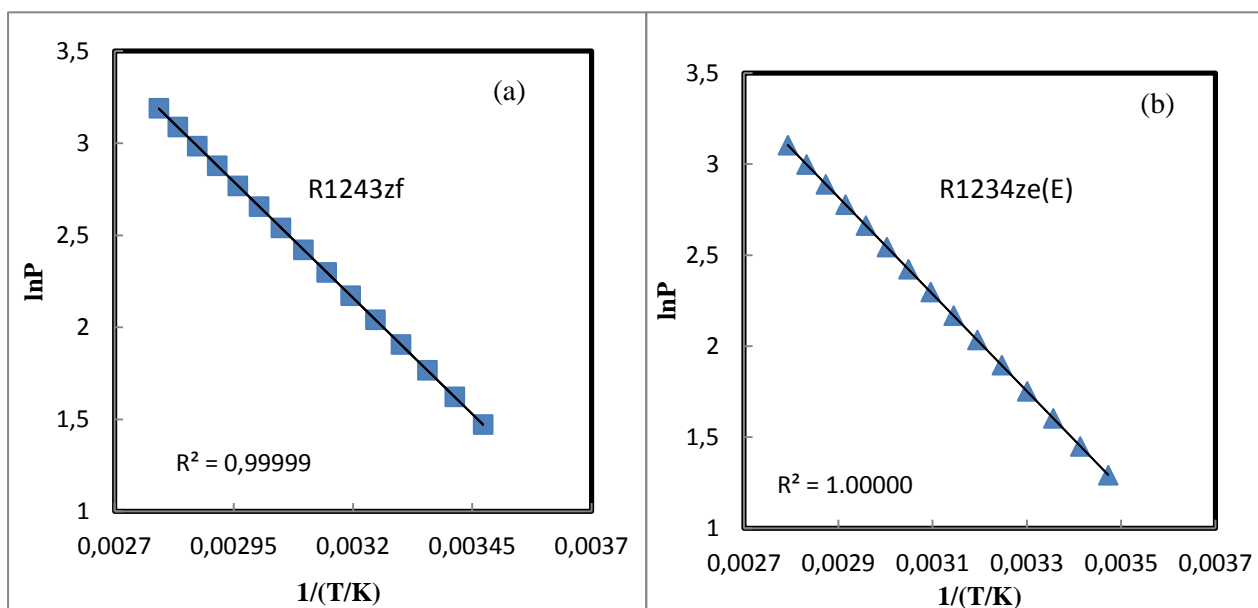


Figure 3. Linear regression for vapour pressure of R1243zf and R1234ze(E) based on Clausius–Clapeyron equation. (a) R1234ze(E); (b) R1243zf; (■): R1243zf; (▲): R1234ze(E).

Table 4. The experimental and calculated vapor pressures of R1234ze(E).

T/K	P_{exp} /MPa	P_{cal} /MPa	ΔP^b /MPa	δp^a /%
288.07	0.3622	0.3619	0.0003	0.09
293.05	0.4245	0.4249	-0.0004	-0.10
298.03	0.4956	0.4957	-0.0002	-0.04
303.01	0.5751	0.5751	0.0000	0.00
308.00	0.6642	0.6640	0.0002	0.03
312.99	0.7630	0.7628	0.0002	0.03
317.97	0.8725	0.8720	0.0004	0.05
322.96	0.9931	0.9926	0.0005	0.05
327.94	1.1259	1.1253	0.0006	0.05
332.92	1.2717	1.2710	0.0007	0.05
337.91	1.4313	1.4309	0.0004	0.03
342.90	1.6055	1.6052	0.0003	0.02
347.89	1.7952	1.7956	-0.0003	-0.02
352.87	2.0017	2.0028	-0.0011	-0.05
357.86	2.2260	2.2280	-0.0020	-0.09

$U(T) = 0.06 \text{ K}$; $U(P) = 0.0004 \text{ MPa}$

$$^a \Delta P = P_{\text{exp}} - P_{\text{ca}}$$

$$^b \delta p = 100 \times (P_{\text{exp}} - P_{\text{cal}}) / P_{\text{exp}}$$

Table 5. The experimental and calculated vapor pressures of R1243zf.

T/K	P_{exp} /MPa	P_{cal} /MPa	ΔP^b /MPa	δp^a /%
288.05	0.4353	0.4349	0.0004	0.10
293.04	0.5061	0.5059	0.0002	0.03
298.03	0.5847	0.5849	-0.0002	-0.04
303.02	0.6727	0.6727	0.0000	0.00
308.00	0.7695	0.7699	-0.0005	-0.06
312.99	0.8769	0.8772	-0.0002	-0.03
317.97	0.9953	0.9952	0.0001	0.01
322.96	1.1252	1.1250	0.0002	0.02
327.94	1.2676	1.2668	0.0007	0.06
332.92	1.4230	1.4218	0.0011	0.08
337.91	1.5924	1.5912	0.0012	0.08
342.90	1.7767	1.7752	0.0014	0.08
347.88	1.9762	1.9758	0.0005	0.02
352.87	2.1929	2.1935	-0.0006	-0.03
357.86	2.4281	2.4298	-0.0016	-0.07

$U(T) = 0.06$ K; $U(P) = 0.0004$ MPa

$$^a \Delta P = P_{\text{exp}} - P_{\text{ca}}$$

$$^b \delta p = 100 \times (P_{\text{exp}} - P_{\text{cal}}) / P_{\text{exp}}$$

According to Clapeyron equation, when vapor-liquid equilibrium is established, $\ln P^{\text{sat}}$ vs. $1/T$ has a linear trend far from critical point according to eq.13.

$$\frac{d \ln P^{\text{sat}}}{d \left(\frac{1}{T} \right)} = - \frac{\Delta H^{lv}}{R \Delta Z^{lv}} \quad 13$$

$$\Delta Z^{lv} = Z^v - Z^l$$

In fact, the vapor-phase compressibility factor Z^v is much larger than that of liquid-phase. Thus Z^l is negligible, and ΔZ^{lv} is equal to Z^v , consequently, a plot of $\ln P^{\text{sat}}$ vs. $1/T$ from experimental data produces nearly straight lines for many substances.

Hence, we use Clapeyron equation as standard to check the accuracy of measurements. As plotted in Figure 3, perfect linear regression is acquired with R^2 equal to 0.99999 and 1.00000 for R1234ze(E) and R1243zf respectively, supporting our vapor pressure data is correct.

The vapor pressures of R1234ze(E) and R1243zf are correlated by PR EoS associated with Mathias-Copeman alpha function (PR-MC EoS), and the regressed parameters are presented in Table 3. The correlation process is performed by a homemade software Tpure which is developed at CTP Mines ParisTech. The calculated vapor pressures of R1234ze(E) and R1243zf are listed in Tables 4 and 5, respectively. Figure 4 shows the relative deviations of vapor pressure correlation, the maximum deviations of R1234ze(E) and R1243zf are both within $\pm 0.1\%$, which shows a good agreement between the experimental data and PR-MC EoS.

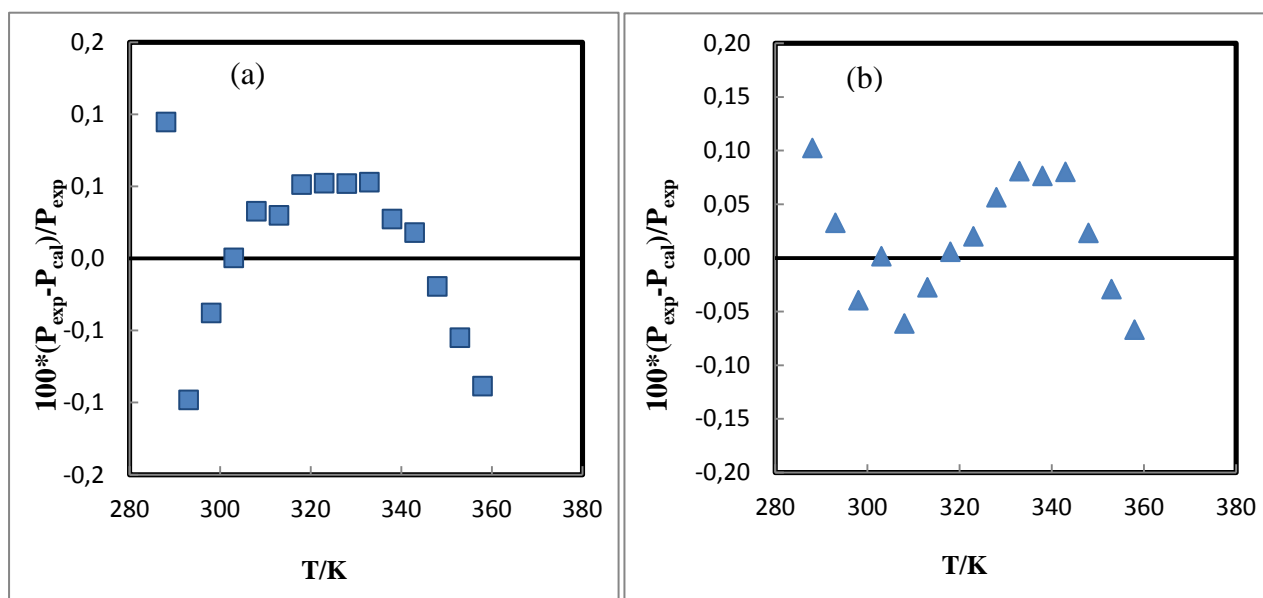


Figure 4. Relative deviations of vapor pressures against PR-MC EoS for R1234ze(E) and R1243zf. (a) R1234ze(E); (b) R1243zf; (■): R1234ze(E); (▲): R1243zf.

4.2. The VLE data of R1243zf + R1234ze(E) system

Vapor-liquid equilibrium of R1243zf + R1234ze(E) binary system is investigated isothermally based on static analytic method at four temperatures, 293.03, 313.02, 332.99, and 352.98 K. The present VLE data of R1243zf + R1234ze(E) system are summarized in Table 6 and plotted in Figure 5. T and P represent the experimental temperature and pressure; n is the number of repeated measurements; x_1 and y_1 are the vapor-phase and liquid-phase mole fraction; $\delta(x_1)$ and $\delta(y_1)$ are the uncertainty of measurement repeatability for

liquid-phase and vapor-phase composition respectively; $u(x_1)$ and $u(y_1)$ are the global uncertainty of mole fraction measurements. Relative volatility with a function of the liquid molar fraction is presented in Figure 6. As it is declined exponentially, we verified the correctness of experimental data.

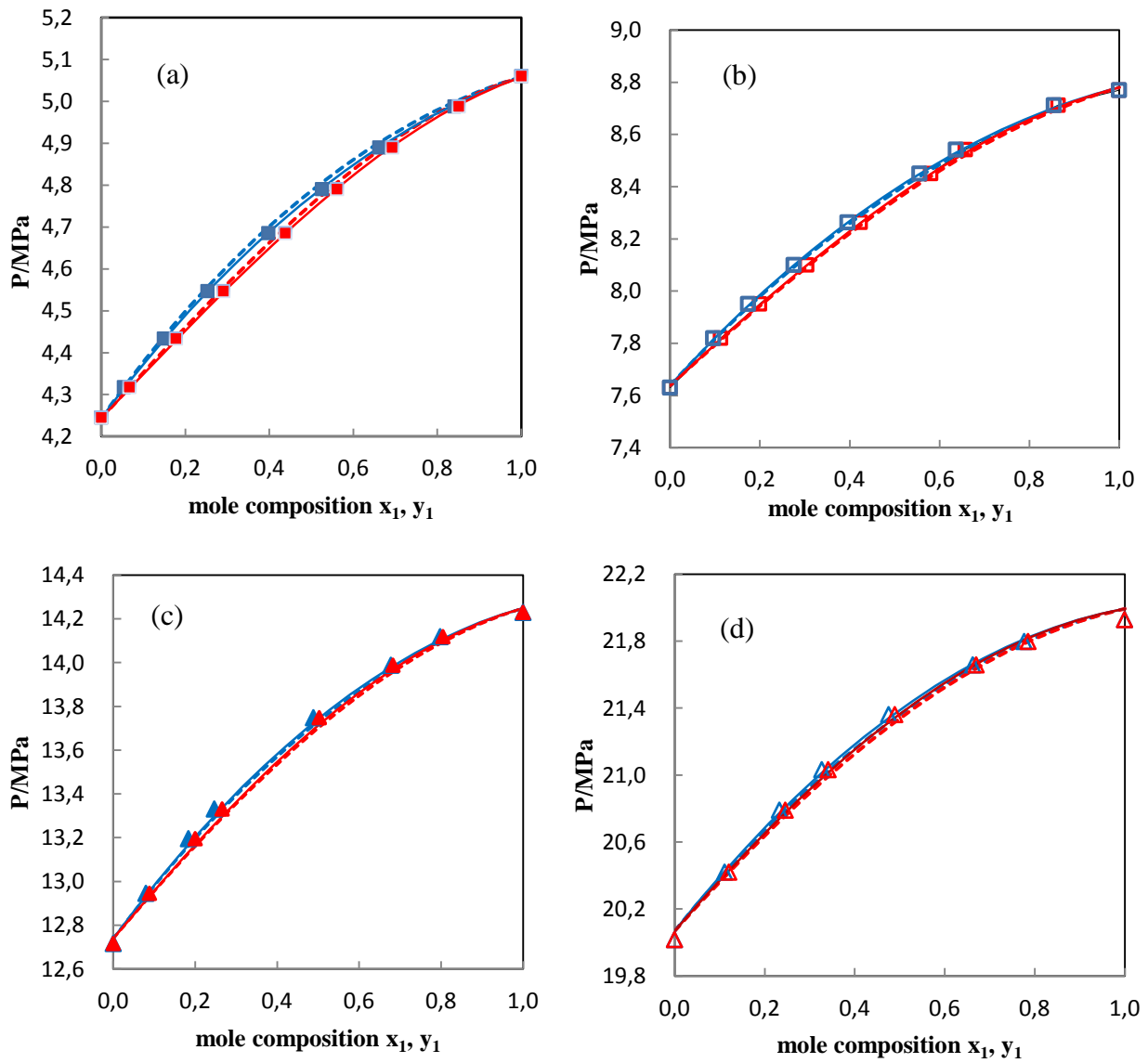


Figure 5. VLE for the R1234ze(E) (1) + 1243zf (2) binary system at different temperatures. (a): 293.03 K; (b): 313.02 K; (c): 332.99 K; (d): 352.98K; (■): 293.03 K; (□): 313.03 K; (▲): 332.99 K; (△): 353.00 K; dash lines: PR-MC-vdW model; solid lines: PR-MC-MHV2 model.

**Table 6. The experimental vapour-liquid equilibrium data of R1243zf (1)+ R1234ze(E)
(2). U(T)= 0.06 K; U(P)= 0.0002 MPa;**

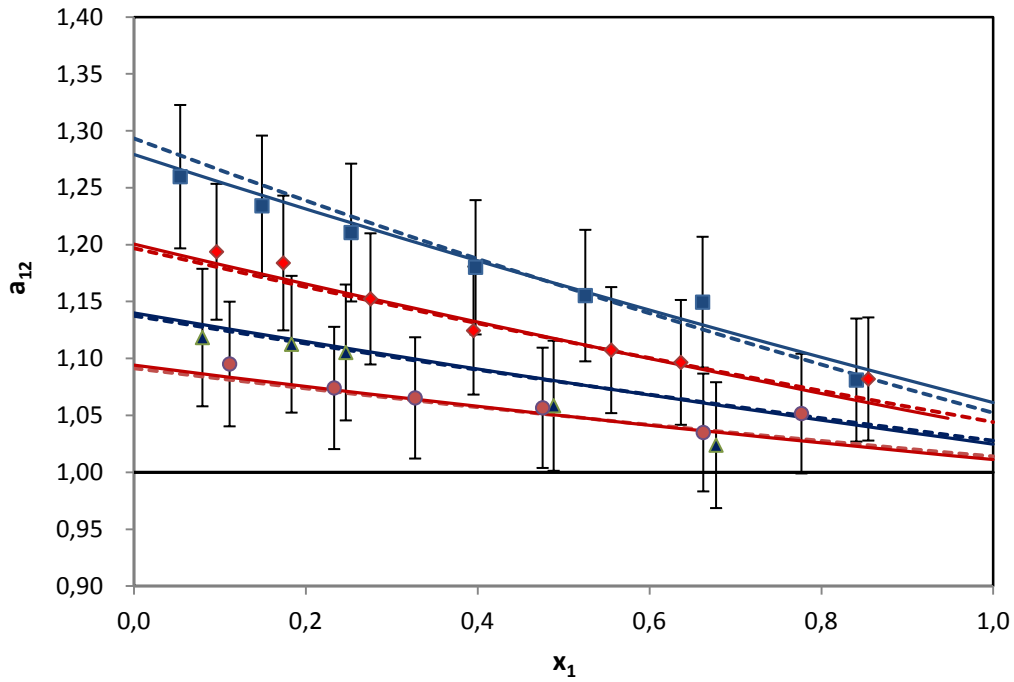
P/MPa	N_x	x_1	$\delta(x_1)$	$u(x_1)$	P/MPa	N_y	y_1	$\delta(y_1)$	$u(y_1)$
T = 293.03 K									
0.4318	6	0.0539	0.0001	0.0006	0.4317	10	0.0669	0.0002	0.0007
0.4434	9	0.1490	0.0002	0.0015	0.4434	8	0.1777	0.0007	0.0017
0.4546	7	0.2528	0.0003	0.0022	0.4548	10	0.2906	0.0002	0.0024
0.4685	7	0.3976	0.0006	0.0028	0.4686	8	0.4379	0.0004	0.0028
0.4790	8	0.5254	0.0015	0.0029	0.4791	12	0.5612	0.0019	0.0028
0.4893	6	0.6619	0.0026	0.0026	0.4887	7	0.6923	0.0006	0.0025
0.4988	7	0.8409	0.0006	0.0015	0.4988	11	0.851	0.0009	0.0015
T = 313.02 K									
0.7820	10	0.0962	0.0006	0.0010	0.7819	12	0.1127	0.0005	0.0012
0.7950	14	0.1739	0.0005	0.0017	0.7951	8	0.1995	0.0008	0.0018
0.8098	8	0.2753	0.0005	0.0023	0.8102	8	0.3045	0.0002	0.0024
0.8263	10	0.3952	0.0011	0.0028	0.8263	8	0.4236	0.0019	0.0028
0.8450	7	0.5555	0.0003	0.0029	0.8450	6	0.5805	0.0014	0.0028
0.8542	8	0.6366	0.0011	0.0027	0.8541	8	0.6577	0.0018	0.0026
0.8712	9	0.8548	0.0013	0.0014	0.8712	6	0.8643	0.0013	0.0014
T = 332.99 K									
1.2948	8	0.0797	0.0004	0.0008	1.2945	9	0.0883	0.0010	0.0009
1.3196	7	0.1835	0.0001	0.0017	1.3196	7	0.2000	0.0008	0.0018
1.3332	10	0.2466	0.0010	0.0021	1.3331	10	0.2657	0.0021	0.0023
1.3750	8	0.4885	0.0012	0.0029	1.3747	9	0.5027	0.0029	0.0029
1.3987	6	0.6776	0.0007	0.0025	1.3989	7	0.6827	0.0006	0.0025
1.4120	8	0.7978	0.0005	0.0019	1.4118	8	0.8046	0.0003	0.0018
T = 352.98 K									
2.0793	7	0.2331	0.0009	0.0021	2.0789	7	0.2461	0.0009	0.0021
2.1033	11	0.3273	0.0004	0.0025	2.1033	10	0.3414	0.0003	0.0026
2.1659	6	0.6627	0.0004	0.0026	2.1658	6	0.6703	0.0004	0.0026
2.1798	8	0.7770	0.0003	0.0020	2.1799	5	0.7856	0.0003	0.0019
2.0420	8	0.1114	0.0001	0.0011	2.0420	8	0.1207	0.0001	0.0012
2.1360	9	0.4757	0.0003	0.0029	2.1363	12	0.4895	0.0022	0.0029

U(T)= 0.06 K; U(P)= 0.0002 MPa; $u_{max}(x_1, y_1)= 0.0029$

1 **Table 7. The experimental and calculated vapour-liquid equilibrium data of R1243zf (1)**
 2 **+ R1234ze(E) (2) at 293.03 to 352.98 K.**

The experimental data			The calculated data							
P _{exp} / MPa	x ₁	y _{1,exp}	PRMC-MHV2-NRTL				PRMC-vdw			
			P _{cal} / MPa	y _{1,cal}	ΔP/ MPa	Δy	P _{cal} / MPa	y _{1,cal}	ΔP/ MPa	Δy
T=293.03 K										
0.4245	0.0000	0.0000	0.4244	0.0000	0.0002	0.0000	0.4244	0.0000	0.0002	0.0000
0.4318	0.0539	0.0669	0.4314	0.0672	0.0003	-0.0003	0.4318	0.0678	0.0000	-0.0009
0.4434	0.1490	0.1777	0.4431	0.1788	0.0003	-0.0011	0.4439	0.1799	-0.0005	-0.0021
0.4547	0.2528	0.2906	0.4546	0.2920	0.0002	-0.0014	0.4557	0.2930	-0.0010	-0.0024
0.4686	0.3976	0.4379	0.4686	0.4392	-0.0001	-0.0013	0.4700	0.4396	-0.0014	-0.0016
0.4791	0.5254	0.5612	0.4793	0.5618	-0.0002	-0.0007	0.4806	0.5615	-0.0016	-0.0004
0.4890	0.6619	0.6923	0.4890	0.6886	0.0000	0.0038	0.4902	0.6878	-0.0012	0.0045
0.4988	0.8409	0.8510	0.4992	0.8524	-0.0004	-0.0014	0.4999	0.8516	-0.0011	-0.0005
0.5061	1.0000	1.0000	0.5059	1.0000	0.0002	0.0000	0.5059	1.0000	0.0002	0.0000
T=313.02 K										
0.7630	0.0000	0.0000	0.7638	0.0000	-0.0008	0.0011	0.7638	0.0000	-0.0008	0.0000
0.7819	0.0962	0.1127	0.7814	0.1118	0.0006	0.0007	0.7811	0.1116	0.0009	0.0011
0.7951	0.1739	0.1995	0.7944	0.1976	0.0007	0.0009	0.7939	0.1972	0.0012	0.0023
0.8100	0.2753	0.3045	0.8099	0.3046	0.0001	0.0001	0.8092	0.3042	0.0008	0.0003
0.8263	0.3952	0.4236	0.8263	0.4254	0.0000	0.0000	0.8254	0.4251	0.0009	-0.0015
0.8450	0.5555	0.5805	0.8449	0.5804	0.0001	0.0001	0.8439	0.5805	0.0011	0.0001
0.8542	0.6366	0.6577	0.8530	0.6572	0.0012	0.0014	0.8520	0.6573	0.0021	0.0003
0.8712	0.8548	0.8643	0.8702	0.8620	0.0010	0.0011	0.8697	0.8623	0.0015	0.0020
0.8769	1.0000	1.0000	0.8780	1.0000	-0.0011	0.0012	0.8780	1.0000	-0.0011	0.0000
T=332.99 K										
1.2717	0.0000	0.0000	1.2739	0.0000	-0.0023	0.0018	1.2739	0.0000	-0.0023	0.0000
1.2946	0.0797	0.0883	1.2935	0.0891	0.0012	0.0009	1.2931	0.0890	0.0015	-0.0007
1.3196	0.1835	0.2000	1.3168	0.2006	0.0028	0.0021	1.3161	0.2003	0.0035	-0.0004
1.3332	0.2466	0.2657	1.3299	0.2664	0.0033	0.0025	1.3290	0.2661	0.0042	-0.0004
1.3749	0.4885	0.5027	1.3725	0.5079	0.0024	0.0017	1.3712	0.5078	0.0037	-0.0051
1.3988	0.6776	0.6827	1.3978	0.6900	0.0010	0.0007	1.3966	0.6902	0.0022	-0.0075
1.4119	0.7978	0.8046	1.4103	0.8050	0.0016	0.0011	1.4094	0.8052	0.0025	-0.0007
1.4230	1.0000	1.0000	1.4249	1.0000	-0.0020	0.0014	1.4249	1.0000	-0.0020	0.0000
T=352.98 K										
2.0017	0.0000	0.0000	2.0069	0.0000	-0.0052	0.0026	2.0069	0.0000	-0.0052	0.0000
2.0791	0.2331	0.2461	2.0774	0.2458	0.0017	0.0008	2.0756	0.2455	0.0035	0.0006
2.1033	0.3273	0.3414	2.1014	0.3411	0.0019	0.0009	2.0991	0.3409	0.0041	0.0005
2.1659	0.6627	0.6703	2.1664	0.6706	-0.0006	0.0003	2.1639	0.6708	0.0020	-0.0005
2.1798	0.7770	0.7856	2.1813	0.7816	-0.0014	0.0007	2.1792	0.7819	0.0006	0.0037
2.0420	0.1114	0.1207	2.0426	0.1195	-0.0005	0.0003	2.0416	0.1193	0.0004	0.0013
2.1362	0.4757	0.4895	2.1341	0.4883	0.0021	0.0010	2.1314	0.4882	0.0047	0.0013

1
2



3
4
5
6
7

Figure 6. Relative volatility for R1234ze(E) (1) + R1243zf (2) binary system. Error bars 5.6%. (■): 293.03 K; (◆): 313.03 K; (▲): 332.99 K; (●): 353.00 K; dashes line: PR-MC-vdW model; solid line: PR-MC-MHV2 model;

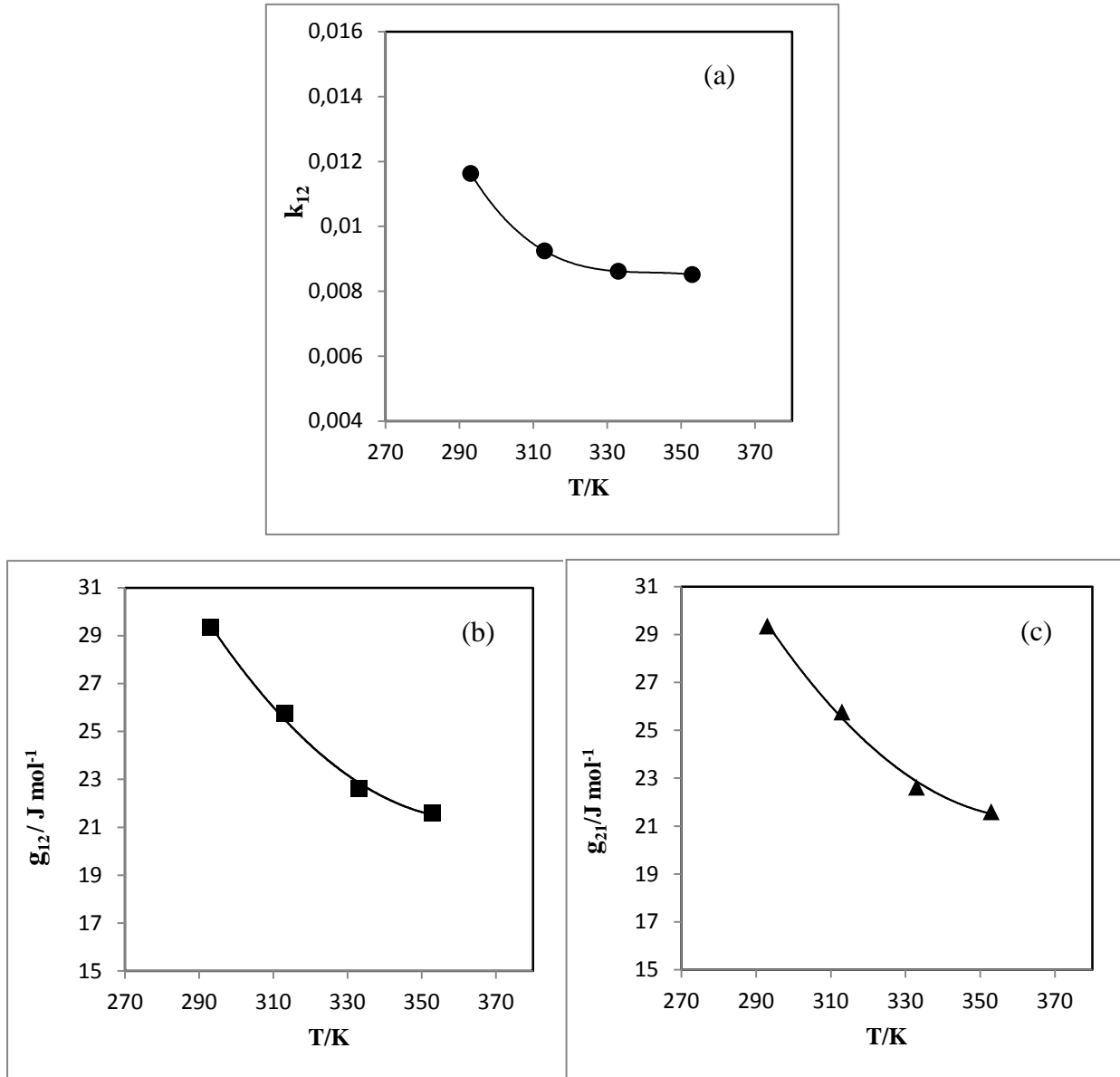
8
9

Table 8. The binary interaction parameters k_{12} adjusted by the model stated as above at each temperature

T/K	PR-MC-vdW						PR-MC-MHV2				
	k_{12}	F	ARDP/%	BIASP/%	AADy	$\Delta g_{12}/\text{J mol}^{-1}$	$\Delta g_{21}/\text{J mol}^{-1}$	F	ARDP/%	BIASP/%	AADy
293.03	0.012	0.0008	0.17	-0.15	0.0014	29.35	29.35	0.0004	0.05	0.01	0.0011
313.02	0.009	0.0005	0.14	0.09	0.0008	25.73	25.76	0.0005	0.08	0.02	0.0008
332.99	0.009	0.0010	0.18	0.12	0.0016	22.61	22.62	0.0010	0.15	0.07	0.0017
352.98	0.009	0.0005	0.14	0.02	0.0009	21.59	21.60	0.0005	0.12	-0.05	0.0008

10
11
12
13
14
15

The VLE data of R1243zf + R1234ze(E) system are correlated by PRMC EoS associated with vdW and MHV2 mixing rules. The regressed binary interaction parameter k_{12} of vdW mixing rules and interaction energy parameters Δg_{12} and Δg_{21} of MHV2 mixing rules are presented in Table 8 and plotted in Figure 7.



1 Figure 7. Variation of the Binary Interaction Parameter (BIP) k_{12} and interaction energy parameters Δg_{12} and
 2 Δg_{21} as a function of temperature for the two models. (a): PR-vdW model; (b, c): RMC-MHV2-NRTL model.
 3 (●): k_{12} ; (▲) Δg_{12} ; (■): Δg_{21} ; Solid line: BIP for PR-vdW model and RMC-MHV2-NRTL model with the
 4 function of temperature.
 5

6 The value of k_{12} , Δg_{12} and Δg_{21} are regressed with a function of temperature. The
 7 fitted results are given in Eq. 14.

$$\begin{aligned}
 k_{12} &= 3 \times 10^{-8}(T/K)^3 + 3 \times 10^{-5}(T/K)^2 - 0.009(T/K) + 1.0334 \\
 \Delta g_{12} &= 0.0016(T/K)^2 - 1.1847(T/K) + 236.69 \\
 \Delta g_{21} &= 0.0016(T/K)^2 - 1.1682(T/K) + 234.04
 \end{aligned}
 \tag{14}$$

8 Figure 5 illustrates the VLE correlations of R1243zf + R1234ze(E) at different

1 temperatures. The R1243zf + R1234ze(E) system shows near-azeotropic refrigerant mixtures
 2 behavior (difference between vapour and liquid compositions values is very low) with
 3 positive deviations from ideality, and the system should exhibits a type I or VI phase
 4 behavior based on the classification scheme of Van Konynenburg and Scott (Coquelet and
 5 Richon, 2009; Konynenburg and Scott, 1980; Privat and Jaubert, 2013). As can be seen from
 6 Fig. 5, the two models give almost the same phase curves. The pressure deviations of
 7 PR-MC-vdW and PR-MC-MHV2 models are presented in Figure 8. The PR-MC-vdW model
 8 shows a lager deviation than PR-MC-MHV2 for all the temperatures. Besides, the
 9 PR-MC-vdW model underpredicts pressures at 293.03 K.

10 To evaluate the accuracy of the VLE models, two statistical indicators, the Average
 11 Relative Deviation (*ARD*) and the Average Bias (*BIAS*) calculated based on pressure and
 12 vapor-composition, are defined in Eqs. 15 and 16.

$$ARDU = \frac{100}{N} \sum_{i=1}^N \frac{|U_{i,exp} - U_{i,cal}|}{U_{i,exp}} \quad 15$$

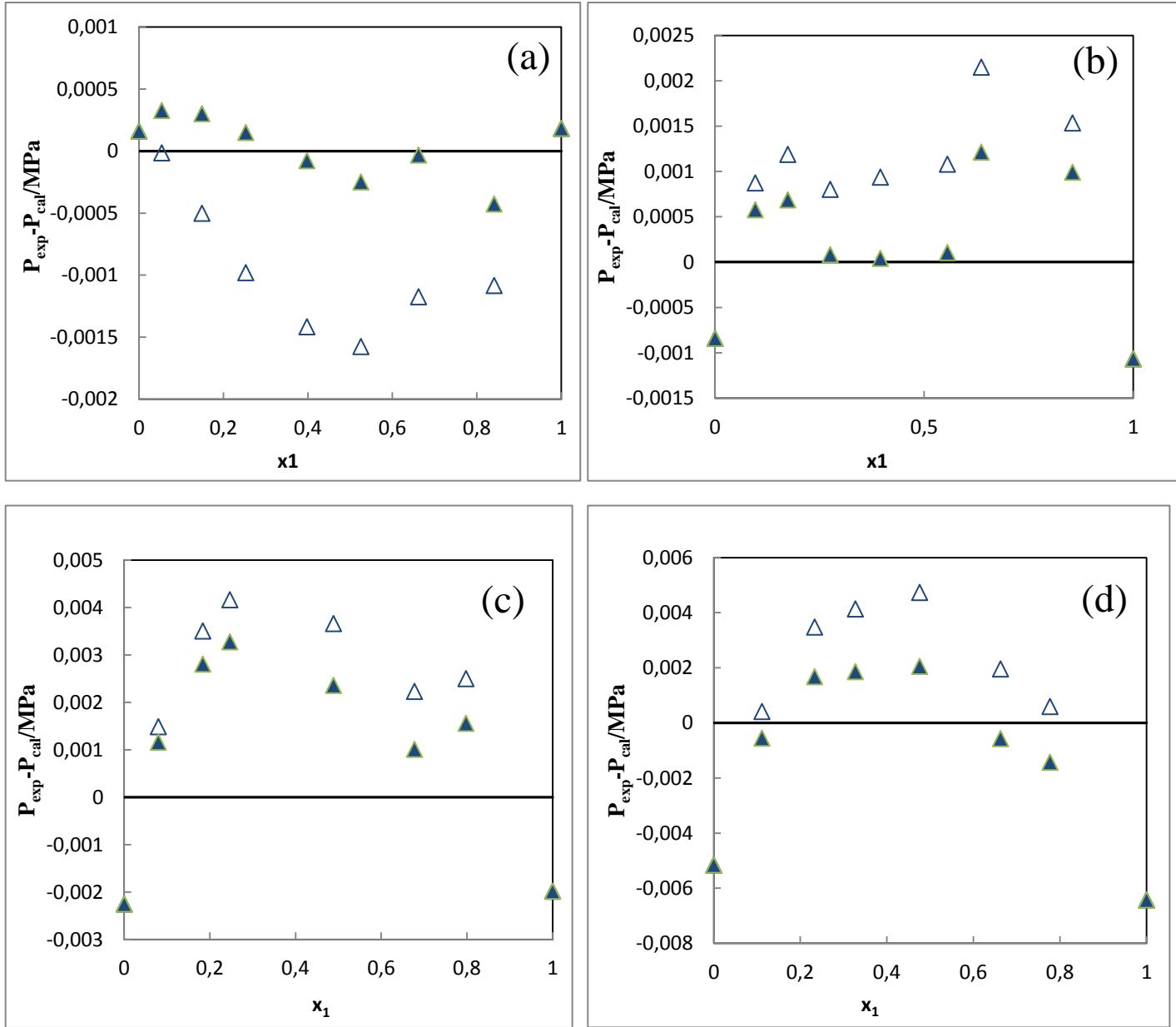
$$BIASU = \frac{100}{N} \sum_{i=1}^N \frac{U_{i,exp} - U_{i,cal}}{U_{i,exp}} \quad 16$$

13 where *N* is the number of experimental points, $U=P$ or y_1 , the subscripts *exp* and *cal* represent
 14 experimental and calculated values respectively.

15 As can be seen in Table 8, all the calculated *ARDP* and *BIASP* of PR-MC-MHV2 model
 16 are smaller than that of PR-MC-vdW model at each isotherm, indicating the MHV2 mixing
 17 rule exhibits much better capability in the representation of VLE behavior for the R1243zf +
 18 R1234ze(E) system.

19 On the consideration of the practical application for the R1243zf + R1234ze(E) binary
 20 mixture, it can be possibly used as working fluid in climatisation system, high temperature
 21 heat pump (HTHP), organic rankine cycle (ORC), and postive refrigeration ($T > 0$ °C). On
 22 the other hand, it's still worthy to investigate VLE behavior at low temperatures, such as the
 23 range from 233 K to 273 K. The best way is to share our data with all community, combined
 24 them with low-temperature VLE data of authors from all the world, that we can model the

1 data in a larger range. However, it still has the possibility to extrapolate the VLE data in
 2 lower temperatures. We can model all the data without temperature dependency. And then
 3 extrapolate the VLE data to the lower temperatures, but need to be careful.



4 Figure 8. Absolute deviation of pressure for the R1234ze(E) (1) + 1243zf (2) binary system from PR-MC-vdW
 5 and PR-MC-MHV2 model. (a): 293.03 K; (b): 313.02 K; (c): 332.99 K; (d): 352.98K; (Δ): PR-MC-vdW model;
 6 (\blacktriangle): PR-MC-MHV2 model.

7

8 Thermodynamic consistency of experimental VLE data is verified based on the point
 9 test method which has presented by Van Ness et al. (1973). That is to calculate y_{cal} from
 10 isothermal $P-x$ data and then to compare the calculated y_{cal} with the experimental value y_{exp} ,

1 here, we define another statistical indicator, Average Absolute Deviation (*AAD*), to test if the
2 VLE experimental data satisfy the thermodynamic consistency.

$$AADy = \frac{1}{N} \sum_{i=1}^N |y_{i,exp} - y_{i,cal}| \quad 17$$

3 *AADy* must be less than 0.01 to obtain thermodynamic consistency (Bertucco et al.,
4 1997). Based on calculated results in Table 8, the *AADy* values at each temperature are less
5 than 1, indicating the thermodynamic consistency was satisfied.

6 **5 Conclusion**

7 Saturated vapor pressures of R1234ze(E) and HFO-1243zf and isothermal vapor-liquid
8 equilibrium of R1243zf + R1234ze(E) binary system are investigated based on static analytic
9 method. The experimental data are given with following uncertainties $U(T) = 0.002 \text{ K}$, $U(P)$
10 $= 0.0006 \text{ MPa}$, and $u_{max}(x_1, y_1) = 0.0029$ for molar composition. The R1243zf + R1234ze(E)
11 binary system exhibits near-azeotropic behavior with positive deviations from ideality. The
12 vapor pressures of R1234ze(E) and R1243zf are well correlated by PR EoS associated with
13 Mathias-Copeman alpha function with relative deviation both within 0.1%. Two
14 thermodynamic models namely PR-MC-vdW and PR-MC-MHV2 are successfully used to
15 represent the VLE of the R1243zf + R1234ze(E) system. The two models give almost the
16 same phase curves and fitted binary interaction parameters are needed to predict the correct
17 phase behavior. However, the PR-MC-vdW model underpredicts pressures at 293.03 K. On
18 the basis of deviations analysis, it has been found PR-MC-MHV2 model exhibits much better
19 capability in the representation of VLE for the R1243zf + R1234ze(E) system.

20

21 Acknowledgment

22 The authors gratefully acknowledge financial support from the China Scholarship
23 Council for Z. Yang's Visiting (No. 201905290003).

24 References

25

- 1 Akasaka, R., 2016. Recent trends in the development of Helmholtz energy equations of state and their
2 application to 3,3,3-trifluoroprop-1-ene (R-1243zf). *Sci. Technol. Built Environ.*
3 <https://doi.org/10.1080/23744731.2016.1208000>
- 4 Akasaka, R., 2010. An application of the extended corresponding states model to thermodynamic
5 property calculations for trans-1,3,3,3-tetrafluoropropene (HFO-1234ze(E)). *Int. J. Refrig.*
6 <https://doi.org/10.1016/j.ijrefrig.2010.03.003>
- 7 Ansari, N.A., Arora, A., Samsher, Manjunath, K., 2020. The Effect of Eco-friendly Refrigerants on
8 Performance of Vapor Compression Refrigeration System with Dedicated Mechanical
9 Subcooling, in: *Lecture Notes in Civil Engineering*.
10 https://doi.org/10.1007/978-981-13-7557-6_4
- 11 Bertucco, A., Barolo, M., Elvassore, N., 1997. Thermodynamic consistency of vapor-liquid
12 equilibrium data at high pressure. *AIChE J.* <https://doi.org/10.1002/aic.690430227>
- 13 Bobbo, S., Nicola, G. Di, Zilio, C., Brown, J.S., Fedele, L., 2018. Low GWP halocarbon refrigerants:
14 A review of thermophysical properties. *Int. J. Refrig.* 90, 181–201.
15 <https://doi.org/10.1016/j.ijrefrig.2018.03.027>
- 16 Boonaert, E., Valtz, A., Brocus, J., Coquelet, C., Beucher, Y., De Carlan, F., Fourmigué, J.M., 2020.
17 Vapor-liquid equilibrium measurements for 5 binary mixtures involving HFO-1336mzz(E) at
18 temperatures from 313 to 353 K and pressures up to 2.735 MPa. *Int. J. Refrig.* 114, 210–220.
19 <https://doi.org/10.1016/j.ijrefrig.2020.02.016>
- 20 Brown, J.S., Di Nicola, G., Fedele, L., Bobbo, S., Zilio, C., 2013. Saturated pressure measurements of
21 3,3,3-trifluoroprop-1-ene (R1243zf) for reduced temperatures ranging from 0.62 to 0.98. *Fluid*
22 *Phase Equilib.* <https://doi.org/10.1016/j.fluid.2012.09.036>
- 23 Brown, J.S., Zilio, C., Brignoli, R., Cavallini, A., 2014. Thermophysical properties and heat transfer
24 and pressure drop performance potentials of hydrofluoro-olefins, hydrochlorofluoro-olefins, and
25 their blends. *HVAC R Res.* 20, 203–220. <https://doi.org/10.1080/10789669.2013.854146>
- 26 Coquelet, C., Richon, D., 2009. Experimental determination of phase diagram and modeling:
27 Application to refrigerant mixtures. *Int. J. Refrig.* <https://doi.org/10.1016/j.ijrefrig.2009.03.013>
- 28 Dahl, S., Michelsen, M.L., 1990. High- pressure vapor- liquid equilibrium with a UNIFAC- based

1 equation of state. *AIChE J.* 36, 1829–1836. <https://doi.org/10.1002/aic.690361207>

2 Di Nicola, G., Brown, J.S., Fedele, L., Bobbo, S., Zilio, C., 2012. Saturated pressure measurements of
3 trans -1,3,3,3-tetrafluoroprop-1-ene (R1234ze(E)) for reduced temperatures ranging from 0.58 to
4 0.92. *J. Chem. Eng. Data.* <https://doi.org/10.1021/je300240k>

5 European Parliament, The Council of the European Union, 2006. Directive 2006/42/EC of the
6 European Parliament and of the Council of 17 May 2006 on machinery, and amending Directive
7 95/16/EC (recast). *Off. J. Eur. Union.*

8 González, S., Jiménez, E., Ballesteros, B., Martínez, E., Albaladejo, J., 2015. Hydroxyl radical
9 reaction rate coefficients as a function of temperature and IR absorption cross sections for
10 CF₃CH=CH₂ (HFO-1243zf), potential replacement of CF₃CH₂F (HFC-134a). *Environ. Sci.*
11 *Pollut. Res.* <https://doi.org/10.1007/s11356-014-3426-2>

12 Higashi, Y., Sakoda, N., 2018. Measurements of PvT Properties, Saturated Densities, and Critical
13 Parameters for 3,3,3-Trifluoropropene (HFO1243zf). *J. Chem. Eng. Data.*
14 <https://doi.org/10.1021/acs.jced.8b00452>

15 Higashi, Y., Sakoda, N., Islam, M.A., Takata, Y., Koyama, S., Akasaka, R., 2018. Measurements of
16 Saturation Pressures for Trifluoroethene (R1123) and 3,3,3-Trifluoropropene (R1243zf). *J.*
17 *Chem. Eng. Data.* <https://doi.org/10.1021/acs.jced.7b00818>

18 Higashi, Y., Tanaka, K., Ichikawa, T., 2010. Critical parameters and saturated densities in the critical
19 region for trans -1,3,3,3-Tetrafluoropropene (HFO-1234ze(E)). *J. Chem. Eng. Data* 55,
20 1594–1597. <https://doi.org/10.1021/je900696z>

21 Juntarachat, N., Valtz, A., Coquelet, C., Privat, R., Jaubert, J.N., 2014. Experimental measurements
22 and correlation of vapor-liquid equilibrium and critical data for the CO₂ + R1234yf and CO₂ +
23 R1234ze(E) binary mixtures. *Int. J. Refrig.* 47, 141–152.
24 <https://doi.org/10.1016/j.ijrefrig.2014.09.001>

25 Katsuyuki, T., 2016. Measurements of Vapor Pressure and Saturated Liquid Density for
26 HFO-1234ze(E) and HFO-1234ze(Z). *J. Chem. Eng. Data.*
27 <https://doi.org/10.1021/acs.jced.5b01039>

28 Kondou, C., Nagata, R., Nii, N., Koyama, S., Higashi, Y., 2015. Surface tension of low GWP

1 refrigerants R1243zf, R1234ze(Z), and R1233zd(E). Int. J. Refrig.
2 <https://doi.org/10.1016/j.ijrefrig.2015.01.005>

3 Konynenburg, P.H. van, Scott, R.L., 1980. Critical lines and phase equilibria in binary van der Waals
4 mixtures. Philos. Trans. R. Soc. London. Ser. A, Math. Phys. Sci.
5 <https://doi.org/10.1098/rsta.1980.0266>

6 Lai, N.A., 2014. Thermodynamic properties of HFO-1243zf and their application in study on a
7 refrigeration cycle. Appl. Therm. Eng. <https://doi.org/10.1016/j.applthermaleng.2014.04.042>

8 Lemmon, E.W., Bell, I.H., Huber, M.L., McLinden, M.O., 2013. NIST Standard Reference Database
9 23: Reference Fluid Thermodynamic and Transport Properties-REFPROP, Version 9.1, National
10 Institute of Standards and Technology 135. <https://doi.org/http://dx.doi.org/10.18434/T4JS3C>

11 Longo, G.A., Zilio, C., Righetti, G., Brown, J.S., 2014. Condensation of the low GWP refrigerant
12 HFO1234ze(E) inside a Brazed Plate Heat Exchanger. Int. J. Refrig.
13 <https://doi.org/10.1016/j.ijrefrig.2013.08.013>

14 Mathias, P.M., Copeman, T.W., 1983. Extension of the Peng-Robinson equation of state to complex
15 mixtures: Evaluation of the various forms of the local composition concept. Fluid Phase Equilib.
16 [https://doi.org/10.1016/0378-3812\(83\)80084-3](https://doi.org/10.1016/0378-3812(83)80084-3)

17 McLinden, M.O., Kazakov, A.F., Steven Brown, J., Domanski, P.A., 2014. A thermodynamic
18 analysis of refrigerants: Possibilities and tradeoffs for Low-GWP refrigerants. Int. J. Refrig. 38,
19 80–92. <https://doi.org/10.1016/j.ijrefrig.2013.09.032>

20 Mendoza-Miranda, J.M., Mota-Babiloni, A., Navarro-Esbrí, J., 2016. Evaluation of R448A and
21 R450A as low-GWP alternatives for R404A and R134a using a micro-fin tube evaporator model.
22 Appl. Therm. Eng. 98, 330–339. <https://doi.org/10.1016/j.applthermaleng.2015.12.064>

23 Mota-Babiloni, A., Navarro-Esbrí, J., Barragán-Cervera, Á., Molés, F., Peris, B., 2015. Experimental
24 study of an R1234ze(E)/R134a mixture (R450A) as R134a replacement. Int. J. Refrig.
25 <https://doi.org/10.1016/j.ijrefrig.2014.12.010>

26 Mota-Babiloni, A., Navarro-Esbrí, J., Barragán, Á., Molés, F., Peris, B., 2014. Drop-in energy
27 performance evaluation of R1234yf and R1234ze(E) in a vapor compression system as R134a
28 replacements. Appl. Therm. Eng. <https://doi.org/10.1016/j.applthermaleng.2014.06.056>

- 1 Orbey, H., Sandler, S.I., 1998. Modeling Vapor-Liquid Equilibria: Cubic Equations of State and Their
2 Mixing Rules. Cambridge University Press.
- 3 Peng, D.Y., Robinson, D.B., 1976. A New Two-Constant Equation of State. *Ind. Eng. Chem. Fundam.*
4 <https://doi.org/10.1021/i160057a011>
- 5 Privat, R., Jaubert, J.N., 2013. Classification of global fluid-phase equilibrium behaviors in binary
6 systems. *Chem. Eng. Res. Des.* <https://doi.org/10.1016/j.cherd.2013.06.026>
- 7 Qiu, G., Meng, X., Wu, J., 2013. Density measurements for 2,3,3,3-tetrafluoroprop-1-ene (R1234yf)
8 and trans-1,3,3,3-tetrafluoropropene (R1234ze(E)). *J. Chem. Thermodyn.* 60, 150–158.
9 <https://doi.org/10.1016/j.jct.2013.01.006>
- 10 Renon, H., Prausnitz, J.M., 1968. Local Compositions in Thermodynamic Excess Functions for
11 Liquid Mixtures. *AIChE J.* 14, 135–143.
- 12 Tanaka, K., Takahashi, G., Higashi, Y., 2010. Measurements of the isobaric specific heat capacities
13 for trans-1,3,3,3-tetrafluoropropene (HFO-1234ze(E)) in the liquid phase. *J. Chem. Eng. Data.*
14 <https://doi.org/10.1021/je900799e>
- 15 UNEP, 2016. The Kigali Amendment to the Montreal Protocol: HFC Phase-down. *OzonAction Fact*
16 *Sheet.*
- 17 Valtz, A., Abbadi, J. El, Coquelet, C., Houriez, C., 2019. Experimental measurements and modelling
18 of vapour-liquid equilibrium of 2,3,3,3-tetrafluoropropene
19 (R-1234yf) + 1,1,1,2,2-pentafluoropropane (R-245cb) system. *Int. J. Refrig.* 107, 315–325.
20 <https://doi.org/10.1016/j.ijrefrig.2019.07.024>
- 21 Van Ness, H.C., Byer, S.M., Gibbs, R.E., 1973. Vapor- Liquid equilibrium: Part I. An appraisal of
22 data reduction methods. *AIChE J.* <https://doi.org/10.1002/aic.690190206>
- 23 Wang, S., Fauve, R., Coquelet, C., Valtz, A., Houriez, C., Artola, P.A., Ahmar, E. El, Rousseau, B.,
24 Hu, H., 2019. Vapor-liquid equilibrium and molecular simulation data for carbon dioxide
25 (CO₂) + trans-1,3,3,3-tetrafluoroprop-1-ene (R-1234ze(E)) mixture at temperatures from 283.32
26 to 353.02 K and pressures up to 7.6 MPa. *Int. J. Refrig.* 98, 362–371.
27 <https://doi.org/10.1016/j.ijrefrig.2018.10.032>
- 28 Wu, X., Dang, C., Xu, S., Hihara, E., 2019. State of the art on the flammability of hydrofluoroolefin

1 (HFO) refrigerants. *Int. J. Refrig.* 108, 209–223. <https://doi.org/10.1016/j.ijrefrig.2019.08.025>
2 Yang, Z., Tang, X., Wu, J., Lu, J., 2019. Experimental measurements of saturated vapor pressure and
3 isothermal vapor-liquid equilibria for 1,1,1,2-Tetrafluoroethane (HFC-134a) +
4 3,3,3-trifluoropropene (HFO-1243zf) binary system. *Fluid Phase Equilib.* 498, 86–93.
5 <https://doi.org/10.1016/j.fluid.2019.06.020>
6

Appendix

Uncertainty analysis of this work

1. Uncertainty of pressure $u(P)$.

The uncertainty of pressure $u(P)$ and uncertainty of temperature $u(T)$ are calculated with the same method. For the $u(P)$, we have two sources of uncertainties, the uncertainty of measurement repeatability ($u_{rep}(P)$) and the uncertainty of calibration ($u_{calib}(P)$). $u_{calib}(P)$ is composed of two terms, $u_{ref}(P)$ and $u_{corr}(P)$. $u_{ref}(P)$ is the uncertainty of the calibrator used. It is obtained from an accredited organism (Laboratoire National d'Essais). $u_{corr}(P)$ is the uncertainty related to the linear or polynomial expression established between the values read on the apparatus used for measurement (pressure transducer) and the values of the calibrator (deadweight balance).

Then, $u(P)$ is calculated by the following formulation (Eq. 1).

$$u(P) = \sqrt{u_{rep}^2(P) + u_{calib}^2(P)} = \sqrt{u_{rep}^2(P) + u_{ref}^2(P) + u_{corr}^2(P)} \quad 18$$

Eq. 2 presents $u_{rep}(P)$ which is a type A uncertainty.

$$u_{rep}(P) = \sqrt{\frac{1}{(N-1)} \sum_{i=1}^N (P_i - P_{avg})^2} \quad 19$$
$$P_{avg} = \frac{1}{n} \sum_{i=1}^n P_i$$

Where P_{avg} is the average of repeated pressure measurements.

Considering our calibration, $u_{ref}(P)$ is negligible and $u_{rep}(P)$ is equal to 0.001 bar.

The uncertainty of correlation (type B) is calculated based on the principle of error propagation. In our case, the linear correlation is utilized for pressure correlation, the $u_{corr}(P) = 0.0004$ bar. Substitute the value of $u_{corr}(P)$ and $u_{rep}(P)$ into Eq. 1, yield $u(P) = 0.0001$ bar. The extended uncertainty on pressure $U(P, k=2)$ is equal to 0.0002 MPa in the range of 0 to 3 MPa.

2. Uncertainty of temperature $u(T)$

The uncertainty of temperature $u(T)$ is calculated by the same method as that of pressure.

The uncertainty of temperature calibrator is $u_{ref}(T) = 0.0006$ K.

The uncertainty of repeatability for temperature measurement is accessed by the calibrated results. Here, we use 8 repeated points at 313.15 K, then substitute into equation 2, yielding $u_{rep}(T) = 0.0035$ K.

The uncertainty of correlation for temperature calibration is $u_{corr}(T) = 0.02$ K. According to Eq. 1, $u(T) = 0.03$ K. The extended uncertainty on temperature is $U(T, k=2) = 0.06$ K in the range of 293 to 393 K.

3. Uncertainty of mole fraction $u(x,y)$

The uncertainty of mole fraction $u(x,y)$ is calculated by Eq.3

$$u(x, y) = \sqrt{u_{rep}^2(x, y) + u_{calib}^2(x, y)} \quad 20$$

Where $u_{rep}(x, y)$ represents the uncertainty of repeatability on liquid-phase or vapor-phase composition measurement, and $u_{calib}(x, y)$ is the uncertainty related to composition calibration.

For the $u_{calib}(x, y)$, it can derive from the definition of mole fraction, which is to calculate mole fraction through a mole number of each compound in the analyzed sample. Mole number and mass are linked by the molar mass.

$$x_1/y_1 = \frac{n_1}{n_1 + n_2}$$

According to the principle of propagation of uncertainty, the combined uncertainty of liquid-phase mole fraction leads to Eq. 4

$$u_{calib}(x_1) = x_1(1 - x_1) \sqrt{\left(\frac{u(n_1)}{n_1}\right)^2 + \left(\frac{u(n_2)}{n_2}\right)^2} \quad 21$$

The relative terms $\frac{u(n_1)}{n_1}$ and $\frac{u(n_2)}{n_2}$ derive from TCD calibration results, and value of $\frac{u(n_1)}{n_1}$ and $\frac{u(n_2)}{n_2}$ are taken as $\frac{1.6\%}{\sqrt{3}}$ and $\frac{.1.2\%}{\sqrt{3}}$.

The $u_{rep}(x_1)$ is the uncertainty of measurement repeatability for liquid-phase

composition which is equal to the standard deviation of repeated composition measurement (δx_1). The uncertainty of mole fraction $u(x_1)$ is calculated by substituting x_1 , δx_1 , $\frac{u(n_1)}{n_1}$, and $\frac{u(n_2)}{n_2}$ into Eq. 3. The δx_1 and $u(x_1)$ at each experimental point are listed in Table 6.

As for the vapor-phase mole fraction, $u_{calib}(y_1)$ and $u(y_1)$ are calculated with the same method. The calculated $u(y_1)$ at each measured point is also listed in Table 6.

As shown in the Table 6, the maximum global uncertainty of composition $u_{max}(x_1, y_1)$ is equal to 0.0029.